ELSEVIER

Journal of Chromatography A, 726 (1996) 1–23

JOURNAL OF CHROMATOGRAPHY A

# Intra-particle sorption rate and liquid chromatographic bandbroadening in porous polymer packings I. Methodology and validation of the model

David Gowanlock, Renata Bailey, Frederick F. Cantwell*

*Department of Chemistry, University of Alberta, Edmonton, Alb., T6G 2G2, Canada*

Received 10 April 1995; revised 14 September 1995; accepted 15 September 1995

**Abstract**

An approach is proposed by which an experimentally measured sorption-rate curve for a solute on a chromatographic sorbent may be used to accurately predict the plate height and peak shape contributions of intra-particle sorption rate to the chromatographic peak that will be obtained when the solute elutes from a liquid chromatographic column of the sorbent. The sorption-rate curve is measured on a "shallow bed" of sorbent (e.g. ≈1 mm) under "infinite solution volume" conditions and is fit by an empirical tri-exponential equation. Intra-particle rate processes include the bandbroadening phenomena traditionally identified by the $H_S$ and $H_{SM}$ plate-height terms. The elution chromatographic column is imagined to be composed of three "hypothetical columns" in series, and the hypothetical peak eluting from each is calculated from well-known equations. Numerical convolution of these hypothetical peaks in series yields the overall predicted elution peak contribution from intra-particle rate processes.

The accuracy of this model is demonstrated by comparing predicted peaks with eluted peaks measured on a long column of very large diameter (0.36 mm) porous polymer sorbent. On this column, chromatographic bandbroadening is due nearly exclusively to slow intra-particle processes. The proposed approach is not limited, either theoretically or in practice, to large particles or to porous polymers.

*Keywords:* Band broadening; Sorption; Stationary phases, LC; Polymer packings, porous; Thermodynamic parameters; Kinetic studies

## 1. Introduction

This series of three papers deals with intra-particle sorption rate in porous polymer chromatographic packings, and its contribution to bandbroadening (including peak shape) in elution chromatography. In the present paper, Part I, an experimental methodology is described for measuring the intra-particle sorption-rate curve, a mathematical model is developed for predicting the contribution of intra-particle sorption rate to peak bandbroadening, and the validity of the model is demonstrated by studies on a very large-particle (non-high performance) packing for which intra-particle sorption rate is the only significant bandbroadening process.

In Part II the experimental method is modified and applied to a microparticle, high-performance LC packing, and the mathematical model is used to predict the contribution of its measured slow intra-particle sorption rate to bandbroadening.

*Corresponding author.

0021-9673/96/$15.00 
*SSDI* 0021-9673(95)01018-1

In Part III it is demonstrated that diffusion through the polymer matrix is the reason why intra-particle sorption rate is slow on the HPLC porous polymer packing.

Porous poly(styrene–divinylbenzene) (PS–DVB) copolymers behave as reversed-phase sorbents in liquid chromatography [1]. Throughout the polymer bead there is present an interconnecting system of permanent macro- and mesopores [2–5]. By convention, pores having widths $\gtrsim$50 nm are called macropores and those having widths between 2 and 50 nm are called mesopores [6,7]. The solid polymer matrix, between the pores, is usually highly crosslinked as a result of a high percentage of DVB in the monomer mix at the time of polymerization [8,9]. However, there may be present in this polymer matrix pores having widths $\lesssim$2 nm which are called micropores [6,7].

In liquid chromatography, PS–DVB packings generally exhibit lower chromatographic efficiencies than do octadecylsilyl (ODS) bonded-phase packings of comparable particle diameter. Of the several possible reasons that have been advanced to explain the lower efficiencies observed on PS–DVB packings, the occurrence of slow processes within the particle seems to have the greatest weight of experimental evidence in its favor [3,10–14].

Any slow behavior of the solute associated with a particle of the chromatographic packing will give rise to reduced column efficiency and, consequently, to a broad and perhaps tailed elution peak for the solute in question [15]. A solute molecule starting in the mobile phase outside of, but near, the particle can experience any or all of the following processes as it is becoming sorbed: "film diffusion" through the quasi-stagnant (Nernst) diffusion film of mobile phase that surrounds the packing particle [16–18]; "pore diffusion" through the stagnant mobile phase that fills the meso- and macropores within the particle [17,19–23]; "surface diffusion" of the adsorbed solute molecule along the surface of the polymer matrix lining the meso- and macropores [20,21]; the "adsorption step" itself in which the solute molecule transfers from the solution in the meso- and macropores onto the surface of the polymer matrix [20,22]; and diffusion into the polymer matrix (perhaps in micropores) [18,20,23]. As the solute is desorbing and leaving the particle it would experience the same processes in reverse.

All of the above steps except the adsorption step involve diffusion and are therefore mass transfer processes. Although, in most adsorbents, the adsorption step is very fast compared to the diffusion steps so that it does not contribute to the observed sorption rate [22–24], it is nevertheless difficult, experimentally, to distinguish adsorption rate-control from mass-transfer rate-control because the rate equations for the two cases are similar to one another [15,22,25].

Another important distinction to be made is that between film diffusion and all of the other steps described above. Taken together, all of these other steps, both diffusive and adsorptive, are responsible for the "intra-particle sorption rate". Experimentally, it is easy to distinguish between film diffusion control and intra-particle control of the overall observed sorption rate [16].

Since previous experimental evidence suggests that it is probably slow intra-particle sorption rate which is responsible for the excessively large chromatographic bandbroadening that is occasionally observed with PS–DVB columns, the goals of the present study are as follows: (1) experimentally measure the intra-particle sorption-rate curve for an aromatic solute being sorbed on a PS–DVB sorbent; (2) describe the observed rate curve mathematically; (3) predict, from the sorption-rate curve, the appearance of the peak that would be obtained for the solute being eluted from a chromatographic column of the PS–DVB sorbent, if intra-particle sorption rate were the only bandbroadening process operating; (4) experimentally test the accuracy of the prediction. Specifically, the rate curve was measured for sorption of the solute 4-phenylazodiphenylamine, from methanol, onto the sorbent Amberlite XAD-2; an elution chromatogram of the same solute was measured on a long column containing the same particle size of XAD-2, using methanol as mobile phase.

## 2. Theory

The approaches and underlying theory relevant to achieving each of the four goals in this study are

described along with several approaches that find currency in the literature.

### 2.1. Measurement of sorption rate

Three different approaches have previously been employed to experimentally measure intra-particle sorption rates on chromatographic packings: column chromatography; spectroscopy; and uptake measurements. In the column chromatographic approach, elution or frontal chromatograms are obtained for the solute on a column of the packing. These are treated in either of two ways. In one treatment, plate heights are calculated from the observed peak or front. The plate heights are plotted versus the linear velocity of the mobile phase and these plots are evaluated in terms of a theoretical equation such as, for example, a van Deemter equation [3,25–32]. In the second type of treatment, statistical moments are calculated for the observed peak or front and these moments are evaluated in terms of theoretical equations relating them to physical properties such as particle size and diffusion coefficients [25,31,33]. The difficulty with all versions of the column chromatographic approach is that the bandwidth and shape of the observed peak or front reflect all of the on-column bandbroadening processes, not just intra-particle sorption rate. Thus, the contributions of effects such as eddy dispersion, mobile-phase mass-transfer resistance and longitudinal diffusion must be subtracted from the overall bandbroadening in order to obtain the intra-particle contribution by difference. The problem of taking differences is compounded when, as is usually the case, the contributions of these other effects are estimated from theoretical equations; but it exists even when the contribution of the extra-particle bandbroadening is measured experimentally [30].

A second approach to experimentally measuring intra-particle sorption rates employs spectroscopic methods. A fluorescence, pressure-jump relaxation method has been used to monitor sorption rate at the surface of a bed of ODS particles filled with mobile phase containing a fluorescent, sorbable solute [34]. A fast relaxation followed by a slower relaxation were interpreted to be related, respectively, to (ad-)sorption of solute on the bonded phase and diffusion of solute into the pores. In a related temperature-jump experiment, the relaxation curve followed a bi-exponential equation and was interpreted in terms of a slow "adsorption" of solute molecule at the surface of the ODS bonded phase followed by a faster "partitioning" of at least a portion of the solute molecule among the ODS chains [35]. While the prospect of separately evaluating the phenomena of surface adsorption, diffusion into the bonded phase, and diffusion into the pores is exciting, at this stage of development the relaxation data cannot be unambiguously interpreted and, furthermore, it is not clear that such techniques are capable of measuring intra-particle processes occurring at locations that are more than only a very short distance from the outer surface of a porous particle.

Another spectroscopic technique, nuclear magnetic resonance, is now routinely used to measure diffusion rates in polymer systems [33]. There are several versions of this technique. The pulsed-gradient spin-echo technique is an important modern one [36]. However, measurement of diffusion in porous polymers represents a challenge to NMR spectroscopy for several reasons: Two or more diffusion coefficients having very different values are often involved; also, measurement of the small diffusion coefficients in porous polymers ($D < 10^{-8}$ cm$^2$/s) requires a high magnetic field.

The last of the commonly-used approaches to experimentally determining intra-particle sorption rates is the uptake-rate measurement, which is performed in either the batch mode or the shallow-bed column mode. In the batch mode a slurry of the sorbent particles is rapidly stirred in a dilute solution of solute dissolved in the proposed mobile phase, and the amount of solute taken up by the sorbent is measured as a function of time [16,20,21,33,37–41]. This measurement can be performed by periodically removing some of the sorbent particles, eluting the sorbed solute and quantifying it; or it can be performed by removing some of the mobile phase, determining the concentration of solute remaining and calculating, by difference, the amount of solute that has been sorbed. A plot of moles of solute sorbed per gram of sorbent versus time is the sorption-rate curve. If the slurry is stirred sufficiently fast the Nernst diffusion layer around the particles

can be made very thin, so that intra-particle sorption processes determine the overall sorption-rate curve [16]. If, during the experiment, the fraction of solute sorbed out of the solution is very small, then solute concentration in the solution is essentially constant and the batch sorption-rate experiment is said to have been performed with an "infinite solution volume" or under "infinite bath" conditions. On the other hand, if the fraction of solute sorbed from the solution is significant, the experiment has been performed with a "finite bath volume" or under "limited bath" conditions [16,21,42]. Naturally, under infinite bath conditions the sorption rate must be monitored in the sorbent phase.

Uptake-rate measurements can also be performed in the "shallow bed" (or "differential reactor") column mode [16,42–47]. In this technique, the sorbent particles are packed as an extremely short bed in a tube. A solution of solute is caused to flow through this shallow bed at a high linear velocity such that, at all times, the concentration of solute in the effluent solution is nearly identical to that in the influent solution and, consequently, all of the sorbent particles in the shallow bed are bathed in a solution containing, essentially, the initial concentration of solute. This creates the equivalent of an "infinite bath" condition. Furthermore, if the linear velocity of solution is high enough, the Nernst diffusion film surrounding the particles in the shallow bed will be very thin so that intra-particle sorption processes will determine the sorption rate. The flow of solution is allowed to proceed for various periods of time, after each of which the amount of solute sorbed is measured. In the present study, the sorption-rate curve is measured under infinite bath conditions using a combination of two versions of the shallow-bed technique.

### 2.2. Equation of the sorption-rate curve

In order to predict the appearance of a peak that would be eluted from a long chromatographic column the sorption-rate curve must first be represented mathematically. There are numerous different expressions that have been developed for this purpose on the basis of theoretical considerations. Theoretically-derived expressions require the assumption of a physical model for the system. The resulting mathematical expressions are cast in terms of physical parameters such as particle diameter, diffusion coefficients, adsorption-rate constants, distribution coefficients, and tortuosity in pores; and they purport to represent the physical processes that are actually taking place inside the particle.

For example, if the particle is considered to be a homogeneous sphere in which diffusional mass transport is rate determining, then in the linear region of the sorption isotherm, well-established equations describe diffusion under either infinite bath or limiting bath conditions, in terms of a single (effective or apparent) diffusion coefficient [16,33,39,43–46,48–50]. The homogeneous sphere may be composed either of a uniform "gel" or of an aggregate of monodisperse "microspheres". Very commonly in the chromatographic literature, the homogeneous spherical diffusion-rate equation is simplified by making the "linear driving force" approximation [16,51,52]. This gives rise, under infinite bath conditions, to a first-order rate expression; and, when used in the rate theory of chromatographic bandbroadening, it gives rise to the often encountered expression of the form:

$$H = \frac{\text{constant}}{60} \frac{d_p^2}{D} U_o \tag{1}$$

where $d_p$ is particle diameter, $D$ is a diffusion coefficient, $U_o$ is linear velocity of mobile phase and $H$ is a plate-height contribution from intra-particle diffusional resistance to mass transfer in porous sorbents, size-exclusion packings and gel-type exchangers [16,17,22,26,27,32,53].

Alternatively, if the sorbent particle is assumed to be bidisperse (or bimodal) it is considered to possess both meso-/macropores and micropores. Theoretically-derived equations usually contain two diffusion coefficients since each of the two pore-size groups is assumed to be homogeneous. The equation may or may not invoke the linear driving force approximation [19,21,23,33,54–56].

If intra-particle sorption rate is controlled by the adsorption step onto a single type of adsorption site,

rather than by mass transfer, the plate height equation has the same form as in Eq. 1, except that the parameter $(d_p^2/60D)$ is replaced by the reciprocal of the first-order desorption-rate constant [19,22,53,57].

Even more-complicated physical models than the ones above can be envisioned involving, for example, parallel pore- and surface-diffusion; heterogeneity either of diffusion coefficients within the micropore region or of adsorption energies among adsorption sites; and simultaneous adsorption and mass transfer-rate control. However, the number of parameters such as diffusion coefficients which need to be independently determined in order to use such models is increased; or, if they are used as fitting parameters, the physical reality of these parameters becomes more tenuous [18,20,33,41,50,58–62].

In the present study a different approach is taken. The equation used to describe the experimental sorption-rate curve is not based on any theoretical model of particle or pore properties. The sorption-rate curve will be fit quantitatively by an equation that is completely empirical. For reasons discussed below, a multi-exponential equation of the form:

$$F = 1 - \frac{n_1}{n_0}\exp(-k_1 t) - \frac{n_2}{n_0}\exp(-k_2 t) - \frac{n_3}{n_0}\exp(-k_3 t)\cdots - \frac{n_i}{n_0}\exp(-k_i t) \qquad (2)$$

must be used, in which $F$ is the fraction of the equilibrium moles of solute that has been sorbed at time $t$ and $n_1$ through $n_i$ are the moles of solute sorbed at equilibrium whose sorption rate can be described by the first-order rate constants $k_1$ through $k_i$, respectively. In the linear region of the solute sorption isotherm the values of $n_1$ through $n_i$ are proportional to the number of type 1 through type $i$ "hypothetical sorption sites" and $n_0$ $(= n_1 + n_2 + \cdots + n_i)$ is proportional to the total number of hypothetical sorption sites on the column. It is important to realize that no physical reality should be attached to the parameters in Eq. 2. It is only in a purely formal sense that there are $i$ different types of sites on the column. When describing the rate curve with Eq. 2, it is not necessary to make any assumptions about pore structure, mass transfer, etc. While there is no guarantee that Eq. 2 will yield a good fit to a given set of experimental data, it is our experience that it usually does so – often as a bi- or tri-exponential equation.

In Fig. 1 is shown the way in which Eq. 2 can be interpreted – though again, only in a formal sense. The experimental data points in Fig. 1 were measured for the sorption of 4-phenylazodiphenylamine solute on the sorbent Amberlite XAD-2, as described later. Duplicate rate experiments, Run nos. 1 and 2,

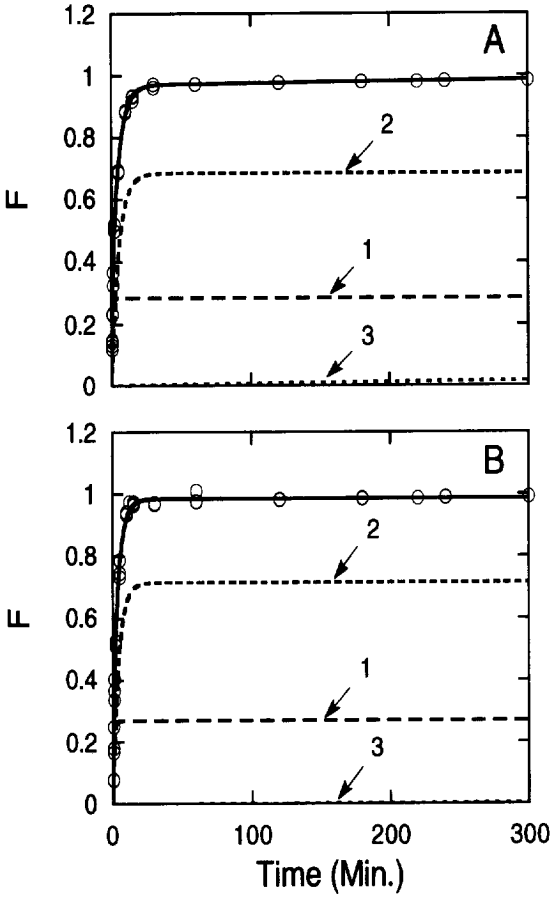


Fig. 1. Sorption-rate curves for 4-PADPA from methanol on XAD-2 under shallow-bed conditions: (A) run 1 and (B) run 2. Circles represent experimental data and solid lines are from non-linear least squares fit to tri-exponential equation (Eq. 2, with $n_i = 3$). Dashed lines are for the three exponential terms. Rate constants $(k_i)$ and equilibrium values $(n_i/n_0)$ for each exponential curve are given in Eq. 17 for (A) and Eq. 18 for (B).

were performed and are shown in Fig. 1A and 1B, respectively. The solid line passing through the points represents the best-fit of the data by Eq. 2 with $n_i = 3$, as obtained by non-linear least-squares curve fitting. The three broken-line curves labeled 1, 2 and 3 in Fig. 1A and 1B correspond, respectively, to the first, second and third exponential terms in Eq. 2, considered individually. At very long times, the limiting values of the solid line and of the other three lines represent the equilibrium values $(n_0/n_0)$, $(n_1/n_0)$, $(n_2/n_0)$, and $(n_3/n_0)$. It can be seen from these curves that in terms of the formalism of Eq. 2, the type 2 hypothetical sites are the most plentiful and the type 3 are least plentiful. The hypothetical rate constant is largest for sorption onto type 1 sites and smallest for sorption onto type 3 sites.

The choice of a sum of exponential terms to describe the sorption-rate curve is essential because, as discussed below, it is possible to predict the shapes of the hypothetical elution peaks that would arise separately from each of the exponential terms in Eq. 2; and furthermore, it is possible mathematically to combine these peak shape contributions in order to predict the elution peak that would arise from the overall sorption rate, Eq. 2. It is most important to realize that, while some other form of empirical equation might conceivably yield a better fit to a set of rate data than is yielded by a multi-exponential equation, that other equation would not be suitable. The proposed approach requires a sum of exponential terms, each with an $n_j/n_0$ and a $k_j$ parameter. The fact that there may even be strong correlations among some of the $n_j$ and $k_j$ parameters does not cause a problem, as shown in Section 4.3.

The advantage of using a purely empirical equation to describe the sorption-rate curve, over attempting to use a theoretically-derived equation based on a physical model, can be seen by comparison with several previously reported studies of sorption rates onto Amberlite XAD-2 and onto the closely related sorbent Amberlite XAD-4. In the previous studies, sorption-rate data from stirred finite-bath experiments [37,50,63] or from shallow-bed (infinite-bath) experiments [45] were fit by equations which assume diffusion into a homogeneous sphere composed of an aggregate of monodisperse microspheres. In two studies, surface diffusion alone was assumed [37,45], in one study parallel surface- and pore-diffusion was assumed [50] and in one study series film- and surface-diffusion was assumed [63]. In most of those studies [45,50,63] sorption-rate curves were measured to within ca. 90 to 95% of the way to equilibrium, so that the presence of very slow uptake in the latter stages, which would necessitate the use of a different model with an extra diffusion coefficient, would be missed. In a study in which long contact times were employed [37], close examination of the data for XAD-2 reveals that a gradual increase in amount sorbed is still taking place at later times; and in a study in which the rate constant for phenol sorption on XAD-4 was used to predict a column breakthrough curve [63], the breakthrough curve shows clear evidence that the homogeneous diffusion model does not adequately describe the latter stages of sorption. In the presently reported work, sorption-rate curves were measured for long times. When the data points from Fig. 1 were fit by the theoretical equation for diffusion into a homogeneous sphere under infinite bath conditions [48] the fit was poor. (It was comparable in appearance to the fit of the light dashed line for the sorbent PRP-1 which is shown in Fig. 1 in Part III of this series.) In contrast, the empirical tri-exponential equation accurately fits the data points in Fig. 1 at all times – short, intermediate and long. Since the purpose of Parts I and II of this series of studies is to accurately predict elution peaks, not to develop a physical model for intra-particle sorption rate, the use of the empirical equation represents a clear advantage. The use of physical models is addressed in Part III, for the HPLC sorbent PRP-1.

### 2.3. Predicted elution peak

Predicting the appearance of an elution peak on the basis of equations describing the rate processes taking place in a chromatographic column is the goal of rate theories of chromatography. To do this the on-column rate expressions must be incorporated into the conservation of mass (mass balance) differential equation for the column and then the differential equation must be solved to give the elution profile (peak) for the solute as it exits the column [16,41,51,52,62,64,65]. In the present case the on-column rate expression of interest is Eq. 2. Giddings and Eyring have shown how the mass

balance equation may be solved for a system which behaves essentially as though it has a *biexponential* sorption-rate equation [66,67]. First, two mass balance equations are solved independently, each containing only one of the two exponential rate expressions from the biexponential equation. This yields two elution profile equations. Then these two elution profile equations are combined by means of the convolution integral in order to obtain the overall predicted elution profile. In the present study this concept is extended to the multi-exponential case, for which $i > 2$ in Eq. 2, by solving the mass balance equations separately, one for each of the exponential terms, and then combining all of the resulting elution profiles by numerical convolution of all of them, in series.

Conceptually, the approach is represented in Fig. 2. When chromatographing 4-phenylazodiphenylamine the column is considered to contain three hypothetical types of sites whose fractional amounts are $n_1/n_0$, $n_2/n_0$ and $n_3/n_0$, as obtained from the limiting values of the broken-line curves in Fig. 1A. In Fig. 2 it is imagined that the three different types of hypothetical sites have been sorted out of the column and collected together by type into three hypothetical columns that are placed in series. These can be referred to generically by the letter $j$, where $j$ is equal to 1 or 2 or 3. Each of the three hypothetical columns has the same length ($L$), linear velocity of mobile phase ($U_o$), retention time of an unretained component ($t_M$), retention volume of an unretained component ($V_M$), and weight of sorbent ($W$), as the real chromatographic column has.

Since the sorption-rate curves and elution chromatograms were measured in the linear part of the sorption isotherm of 4-phenylazodiphenylamine, the distribution coefficient for this solute on the real column is a constant, $K_D$, which has the units $(\text{mol/site})(\text{mol/l})^{-1}$. On the real column the phase ratio is $\phi$ with units of sites per liter.

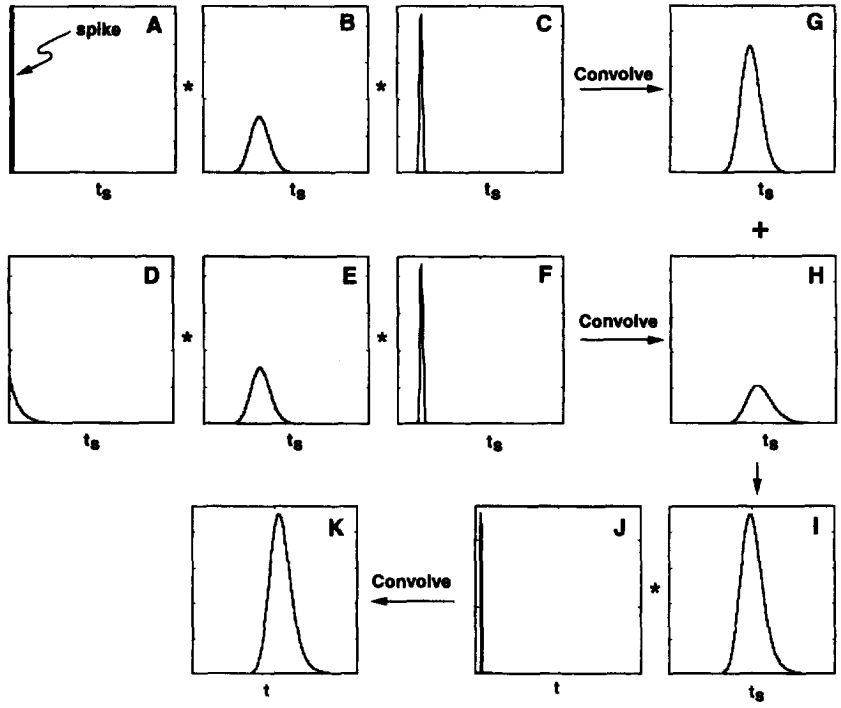


Fig. 2. Steps in predicting an elution chromatographic peak (panel K): The peaks predicted to elute from each of the three hypothetical columns ($j = 1$, 2 and 3) for the fraction that is not sorbed on $j = 3$ (panels A, B and C) are convolved to give G; and the peaks predicted to elute from the same three hypothetical columns for the fraction that is sorbed on $j = 3$ (panels D, E and F) are convolved to give H. The resulting peaks in G and H are added to give I. Convolution of I with J gives K.

The capacity factor, $k'$, for the solute on the real column is:

$$k' = K_D \phi \tag{3}$$

The capacity factor $k'_j$ for the solute on any one of the hypothetical columns $j$ is:

$$k'_j = K_D \phi \frac{n_j}{n_0} \tag{4}$$

Consequently, $k'$ on the real column is related to $k'_j$ by the expression

$$k' = \sum_{j=1}^{i} k'_j \tag{5}$$

The rate constant for hypothetical column $j$, obtained from fitting Eq. 2 to the sorption-rate data, is $k_j$. For reversible first-order sorption this rate constant is related to an adsorption-rate constant $k_{a,j}$ and a desorption-rate constant $k_{d,j}$ by the expression [22]:

$$k_j = k_{a,j} + k_{d,j} \tag{6}$$

These adsorption and desorption-rate constants are also related to the capacity factor by the expression:

$$k'_j = \frac{k_{a,j}}{k_{d,j}} \tag{7}$$

Combining Eqs. 3, 4, 6 and 7 relates the adsorption and desorption-rate constants to both the rate constant from the $j$th term in Eq. 2 and the $k'_j$ for hypothetical column $j$:

$$k_{a,j} = k_j \frac{k'_j}{1 + k'_j} \tag{8}$$

$$k_{d,j} = k_j \frac{1}{1 + k'_j} \tag{9}$$

If an impulse of solute is injected onto any one of the three hypothetical columns alone, the resulting hypothetical elution peak can be predicted as follows [22,66,67]. First, there may be some significant portion of the solute molecules, $P'(t_S)$, that will pass through the column without being sorbed at all. If so, they will appear as a spike at time $t_M$ which is described by the expression:

$$P'(t_S) = \delta(t_S) \exp(-k_{a,j} t_M) \tag{10}$$

Here $\delta(t_S)$ is the Dirac impulse function, which is an infinitely narrow pulse. The choice of units for $\delta(t_S)$, e.g. moles of solute injected, will establish the units for $P'(t_S)$, e.g. moles of solute eluted at time $t_M$. The exponential term in Eq. 10 is the fraction of solute molecules that are never sorbed. For the molecules that *are* sorbed during their transit through hypothetical column $j$ (i.e. $1 - P'(t_S)$), the elution profile (peak shape) is given by:

$$P(t_S) = \left(\frac{k_{a,j} k_{d,j} t_M}{t_S}\right)^{1/2} I_j\left(\sqrt{4 k_{a,j} k_{d,j} t_M t_S}\right) \times \exp(-k_{a,j} t_M - k_{d,j} t_S) \tag{11}$$

Here $I_j$ is a Bessel function of imaginary argument for the parenthetic square-root term [68]. Eqs. 10 and 11 are expressed in terms of the elapsed-time variable $t_S$ which is measured with $t_M$ taken as zero ($t_S = t - t_M$).

The predicted hypothetical elution peaks for 4-phenylazodiphenylamine on Amberlite XAD-2 are shown in Fig. 2. Panels B and E both show the same peak which is predicted for hypothetical column 2; panels C and F both show the same peak which is predicted for hypothetical column 1; panel A shows the spike predicted from Eq. 10, and panel D shows the peak predicted from Eq. 11, both for hypothetical column 3. Panel G shows the result of mathematically convolving the peaks in panels A, B and C with one another. Panel H shows the result of convolving the peaks in panels D, E and F with one another. The relative areas of the peaks in panels G and H are scaled in the ratio $P'(t_S)/(1 - P'(t_S))$. The peak in panel I is the sum of the peaks in panels G and H. In order to obtain the final peak which is predicted to elute from the end of the real chromatographic column, the peak in panel I must be convolved with the real peak at $t_M$ which is obtained upon elution of an unretained component ($k' = 0$) from the real chromatographic column. The unretained component peak is shown in panel J. This final convolution step has the effect of shifting the center-of-gravity of the peak in panel I along the time axis by an amount $t_M$ and of increasing its variance by an amount equal to the variance of the unretained-component peak. While the peaks shown in panels A through I are hypothetical, the peaks in panels J and K are not. The peak shown in panel K is the one that is

predicted to elute from the real chromatographic column. (In the present case, the variance of the unretained-component peak in panel J (i.e., $\approx 9\times10^{2}$ $min^2$) would be negligibly small in comparison to the variance of the peak in panel I (i.e., $\approx 6\times10^{5}$ $min^2$), so that the only noticeable effect of convolving I with J to produce K is to add $t_M$ to the center of gravity of I.)

In order to perform the calculations just described it is necessary to have experimentally-based values for $t_M$ and $k'$ that are relevant to the chromatographic column that is packed with the sorbent in question. The relevant $t_M$ value for a column which has length $L$ and linear velocity $U_o$ is $t_M = L/60U_o$. The relevant $k'$ value can be obtained in either of two ways: It may be obtained by running an experimental elution chromatogram of the solute and making the usual calculation:

$$k' = \frac{V_R - V_M}{V_M} = \frac{t_R - t_M}{t_M} \tag{12}$$

Here it is important that the retention volume $V_R$ or time $t_R$ be taken as the center-of-gravity of the peak [60,69]. Alternatively, $k'$ can be estimated, without running a chromatogram, from the equilibrium plateau value $n_0$ in the shallow bed rate experiment, using the expression:

$$k' = \frac{n_0 - C_M V_{pore}}{W_{SB} C_M} \frac{W_{col}}{V_M} \tag{13}$$

where $W_{SB}$ and $W_{col}$ are the weights of sorbent in the shallow bed and in the chromatographic column, respectively; $C_M$ is the concentration (mol/l) of solute in the solution flowing through the shallow bed; $V_{pore}$ is the intra-particle pore volume in $W_{SB}$ grams of sorbent; and $V_M$ is the retention volume of an unretained component on the chromatographic column. The product $C_M V_{pore}$ is subtracted from $n_0$ in this equation because $n_0$ includes the solute in the stagnant mobile phase filling the pores of the sorbent particles in the shallow bed. Use of Eq. 13 to obtain $k'$ requires accurate knowledge of $W_{col}$. In a prepacked column $W_{col}$ may not be known.

Extension of the Giddings two-site model as described here bears only a superficial resemblance to the highly theoretical extension to $n$-sites presented by McQuarrie [70] and to the inferential extension to three-sites as presented by Vint and Philips [71]. In neither of these two treatments are the relevant kinetic parameters measured in a separate sorption-rate experiment, and in both of them the kinetic parameters are implied to have physical reality. The present treatment is, in fact, more similar to the approach of Villermaux [60,69] who imagined hypothetical columns of different lengths to be placed in series. However, in Villermaux's approach the "transfer function" which is used to describe mass transfer, while not formulated in terms of diffusion coefficients and other physically meaningful parameters, nevertheless is derived from chromatographic measurements and is therefore tied to the chromatographic experiment in a way that the $n_j$ and $k_j$ parameters in the present model are not.

### 2.4. Accuracy of predicted peak

The only bandbroadening processes that are taken into account in predicting the elution peak from Eqs. 10 and 11 are intra-particle processes. In the terminology of chromatographic rate theory, these intra-particle processes are resistance to mass transfer in both the stagnant mobile phase and the stationary phase [15–19,26,32,53]. Plate height contributions associated with these are $H_{SM}$ and $H_S$, respectively [53]. The other generally accepted bandbroadening processes are sometimes classified as longitudinal diffusion in the mobile phase ($H_{LD}$), eddy dispersion ($H_E$) and resistance to mass transfer in the (flowing) mobile phase ($H_M$). Thus, the peak that is predicted in the proposed approach, on the basis of the measured intra-particle sorption-rate curve, is the peak that would be expected from a chromatographic column for which intra-particle processes are the only ones giving rise to bandbroadening. If other bandbroadening processes are also operative on a chromatographic column, then the observed chromatogram would be a convolution of this predicted peak with the peaks arising from the other bandbroadening effects.

For this reason, when comparing the peak predicted from Eqs. 10 and 11, as described in Fig. 2, with a peak measured experimentally, for the purpose of validating the proposed approach, it is necessary that the experimental peak should be measured under conditions where all other contribu-

tions to bandbroadening are negligible compared to intra-particle sorption rate. In order to achieve these conditions very large particles of sorbent were used. As a consequence of using such large particles, a very low linear velocity of mobile phase and a rather long column had to be used in order to achieve a reasonably large number of plates. Also, a solute having a large $k'$ was employed to minimize experimental uncertainties associated with measuring the sorption-rate curve in the shallow bed experiment.

Experimental validation of the proposed approach to predicting the elution peak requires that the same solute, mobile phase and sorbent (including particle size) are used in both the shallow bed and the elution chromatographic experiments. The observed peak is compared with the predicted peak by direct visual comparison and by comparison of chromatographic figures of merit.

## 3. Experimental section

### 3.1. Reagents and chemicals

4-Phenylazodiphenylamine (4-PADPA) (97%, Eastman Kodak) was recrystallized from 40% methanol–water. Phloroglucinol (1,3,5-trihydroxybenzene, Fisher) was recrystallized from water. *o*-Nitroaniline (98%, Aldrich) was used as received.

Doubly distilled and deionized water from a nanopure filtration/distillation system (Barnstead Co.) was used throughout, except where otherwise noted. Methanol was distilled reagent grade (BDH, 99.8%) and was filtered through a 0.45-$\mu$m Nylon 66 membrane filter prior to use.

For the shallow-bed sorption rate measurements a solution containing approximately $4\times10^{-5}$ mol/l of 4-phenylazodiphenylamine in methanol was used. This concentration is in the linear region of its sorption isotherm. A solution of phloroglucinol in methanol was used to measure the hold-up volume of the shallow bed.

### 3.2. Sorbent

Nominally 20–50 mesh Amberlite XAD-2 (Fisher Scientific, Lot No. 2-0218) was dry sieved. The material was taken which passed a 40-mesh (420 $\mu$m) sieve and was retained on a 60-mesh (250 $\mu$m) sieve. About 1300 g of this material was then subjected to solvent elutriation as described below. The yield was 630 g of dry XAD-2 which, from microscopic measurement of 224 individual particles, was found to be composed of spherical and somewhat elipsoidal particles having a mean Martin's "accidental" diameter [72] of 360±31 $\mu$m. This material was washed in a funnel with methanol, with 1.2 *M* HCl and with water to neutrality. It was then dried in vacuo at 80°C for three hours. This 360±31 $\mu$m cut of XAD-2 was used in all studies reported in this paper.

### 3.3. Apparatus

Solvent elutriation was performed in a water-jacketed glass column thermostatted at 25±1°C. The elutriation column had a total length of 50 cm. The upper 30 cm had parallel walls with an internal diameter of 5 cm. The lower 20 cm was tapered uniformly to an I.D. of 0.8 cm at the lower end. Below this was a 15-cm long by 0.8-cm I.D. extension that terminated in a 1-l water-filled flask by means of an air-tight connector. Water elutriant, pre-equilibrated at 25±1°C entered near the bottom of the tapered section at a flow-rate which was maintained constant by means of a constant hydrostatic head. The slurry of XAD-2 in water was fed continuously at a slow rate. Other features of the design and operation of the solvent elutriation apparatus are similar to those previously described [72].

The shallow-bed apparatus, which was used to measure sorption rates at times up to 30 min is shown in Fig. 3. P1, P2 and P3 are constant-pressure pumps of a type previously described [73]. Valves $V_1$ and $V_2$ are a six-port rotary valve and a three-way slider valve, constructed from Teflon and Kel-F (Cheminert, Chromatronix Corp.). Valve $V_3$ is a Cheminert sample injection valve (Model SV 8031) fitted with a 2.3-ml loop of Teflon tubing to serve as a holding loop. Components F1 and F2 are in-line filters employing porous Teflon membrane filter elements. Component S is a Model UV50 spectrophotometric liquid chromatography detector (Varian); I is a Vista CDS 401 integrator (Varian); P4 is a

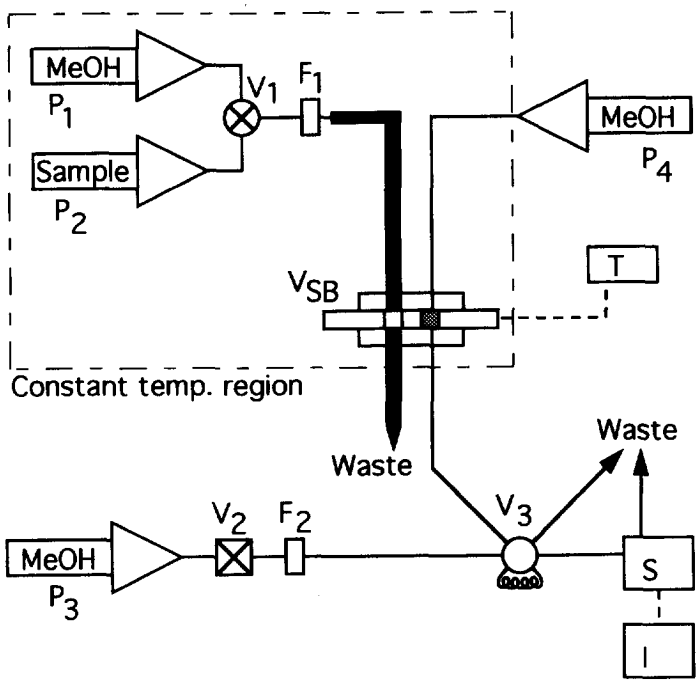


Fig. 3. Shallow-bed apparatus for measuring intra-particle sorption rate. $P_1$–$P_4$: pumps; $V_1$–$V_3$: valves; $F_1$ and $F_2$ are in-line filters; T is a valve-position timer; S is an HPLC photometric detector; and I is an integrator. The valve $V_{SB}$ contains the shallow-bed of XAD-2. An enlargement of $V_{SB}$ is shown in Fig. 4. See text for details.

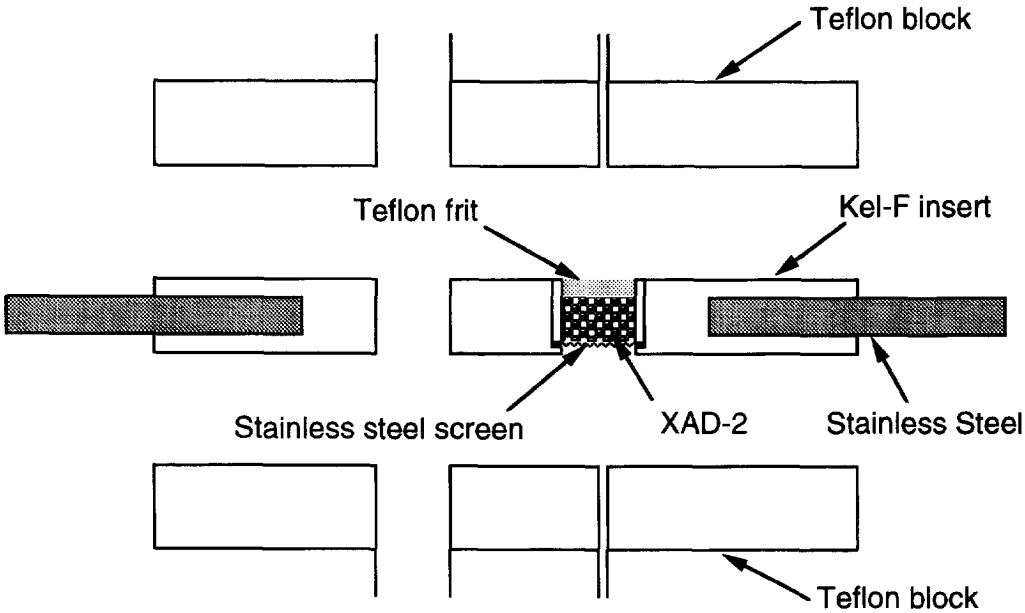


Fig. 4. Enlargement of the main components of the shallow-bed valve $V_{SB}$, shown disassembled. The bed of XAD-2 is approximately 1-mm high and 3.0-mm diameter. The left-hand entry- and exit-tubes are also 3.0 mm I.D. to facilitate a uniform flow of sample solution during the sorption step. See text for details.

homemade syringe pump constructed from a Manostat microburet and a stepping motor. Component T is a Model 5321B electronic counter (Hewlett-Packard) that is used as a timer in conjunction with a magnetic switch attached to the body of the shallow-bed valve, $V_{SB}$. The timer is activated when the slider is pushed to the left so that the shallow bed is in the sample solution flow stream, and timing stops when the slider is pushed back to the right-hand position. The slider (Fig. 4) consists of a 3.6 cm×1.3 cm×1.4 mm flat piece of stainless steel, the centre of which is cut out and holds a 2 mm high×2.9 cm×1.1 cm piece of Kel-F with two 3-mm diameter holes drilled through it. The hole on the left is empty and the hole on the right contains a stainless steel screen at the bottom. On this screen is the bed of XAD-2 (ca. 3.5 mg, accurately weighted) which is about 1 mm high. On top of the bed is a force-fit 3-mm diameter disk of porous Teflon (Zitex, K1064-222, 30–60 $\mu$m pore size, Chemplast, Wayne, NJ, USA). The left-hand tubes entering the top and leaving the bottom of $V_{SB}$ have the same internal diameter as the bed of XAD-2 (3 mm) in order to insure uniform flow through the bed which facilitates the achievement of "shallow-bed conditions" during the sorption step. The right-hand inlet and outlet tubes are 0.5 mm I.D. Elution of the sorbed 4-PADPA from the XAD-2 does not require shallow-bed conditions. The shallow-bed apparatus was thermostatted at 25±1°C by immersion in a constant-temperature bath (Blue M Corp.)

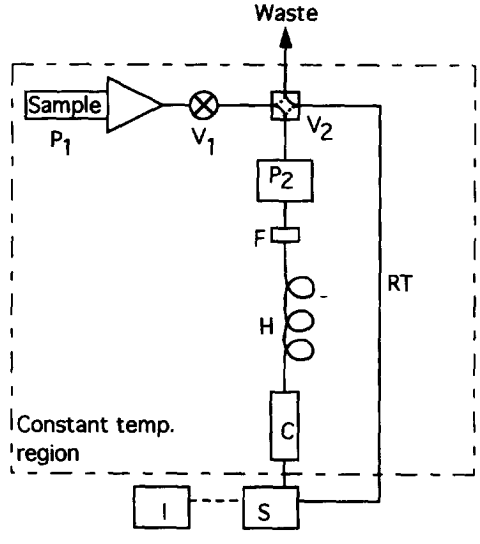


Fig. 5. Recirculation apparatus for measuring sorption rates at times greater than 30 min. $P_1$ and $P_2$ are pumps; $V_1$ and $V_2$ are valves; H is a heat-exchanger tube; RT is a recirculation tube; and C is a glass column containing a 3 cm×3-mm I.D. bed of XAD-2. See text for details.

The recirculation apparatus which was used to measure sorption rates at times greater than 30 min is pictured in Fig. 5. The column, C, consists of a 3 cm×3 mm I.D. glass tube containing 61.9 mg of XAD-2 held between two disks of porous Teflon (Zitex). $V_1$ is a six-position Cheminert rotary valve. P1 is a constant pressure pump and P2 is a peristaltic pump (Ismatec) employing a Viton rubber pump tube. F is an in-line filter. H is a heat exchanger located upstream of the detector, which consists of 50 cm of 0.5 mm I.D. stainless steel tubing. S is a UV50 HPLC detector and I is the Vista integrator. The recirculation tube, RT, is a Teflon tube that connects the outlet of the detector with the four-port Cheminert valve, $V_2$. When $V_2$ is in the position shown with solid lines, and the rollers on the peristaltic pump are released, P1 pumps fresh 4-PADPA solution through the entire system and to waste. In the second position, shown with dashed lines, $V_2$ creates a closed recirculation loop within which the peristaltic pump recirculates the sample solution through the column and detector. The apparatus was thermostatted by immersion in a constant-temperature bath.

The elution chromatograph was used to measure the (observed) chromatographic peak of 4-PADPA eluted with methanol mobile phase. The column consisted of a bed of XAD-2 (51×1.27 cm) that was dry-packed in a precision-bore glass tube using the "tap-fill" technique [74]. An adjustable plunger (Cheminert, Chromatronix Inc.) at the top of the bed insured that it was flat. Visual observation of the injected unretained dye *o*-nitroaniline revealed that the bed exhibited trans-column uniformity of axial linear velocity, even at the very top. Methanol eluent was supplied from an elevated 2-l reservoir. A Cheminert rotary injection valve with a 1.5-ml injection loop was positioned between the reservoir and the column. The flow-rate of methanol was accurately controlled with a peristaltic pump

(Minipuls 2, Gilson) located downstream of the column. A fraction collector (Buchler Fractomette alpha 200) was used to collect the column effluent. The amount of 4-PADPA in each fraction was determined by evaporating to dryness, dissolving the residue in 5.00 ml of methanol and measuring absorbance at 408 nm.

### 3.4. Procedures

Solvent elutriation of the screened XAD-2 was performed first at a water flow-rate of 150 ml/min. The particles which settled into the 1-l flask at this flow-rate were re-introduced into the column at a flow-rate of 180 ml/min. The particles leaving the top of the column had a diameter of 360±31 $\mu$m. These were the particles used in all experiments.

Sorption-rate measurements employing the shallow bed (Fig. 3 and Fig. 4) involved the following steps. (i) Pre-equilibration: the bed was rinsed by flowing methanol through it for about 1 h; (ii) Flushing: with the shallow bed in the right-hand position in $V_{SB}$ (as shown in Fig. 3) valve $V_1$ was switched to allow at least 15 ml of the sample solution of 4-PADPA in methanol to flush the system; (iii) Sorption: at time $t = 0$ the shallow bed was switched to the left-hand position in $V_{SB}$, where it was left for accurately-timed periods ranging from 15 s to 30 min; (iv) Desorption: at the end of the sorption step the shallow bed was switched back to the right-hand position where pure methanol from pump P4 desorbed and eluted the 4-PADPA at a flow-rate of 0.100 ml/min. The desorbed 4-PADPA was either passed directly through $V_3$ to the UV50 detector as a peak or it was collected in the Teflon holding loop in $V_3$ and subsequently rinsed through the UV50 detector as a peak using a flow-rate of 0.182 ml/min of methanol from pump P3. The area of the peak in either case served for quantitation against a calibration curve obtained by filling the holding loop of $V_3$ with standard solutions of 4-PADPA and injecting them through the detector at the same flow-rate.

Calculation of the concentration of 4-PADPA sorbed at a given time in the shallow-bed experiment is performed via the following expression:

$$C_S = \frac{n_T - C_M(V_{HU} - V_{pore})}{W_{SB}} \quad (14)$$

in which $C_S$ is moles 4-PADPA sorbed per gram of XAD-2. $C_M$, $V_{pore}$ and $W_{SB}$ are as in Eq. 13. $C_M$ for 4-PADPA is a constant concentration in the shallow-bed experiment. $V_{HU}$ is the hold-up volume of the shallow bed, which includes all liquid-filled spaces in the right-hand slider hole depicted in Fig. 4. $V_{HU}$ is measured by equilibrating the shallow bed with a methanol solution of the unretained compound phloroglucinol, desorbing and measuring the amount of phloroglucinol in the bed. A typical value of $V_{HU}$ is 10.13±0.02 $\mu$l for the bed used in run 1. $V_{pore}$ is obtained by combining the skeletal density (1.07 g/ml) and intra-particle porosity (0.43 ml/ml) of XAD-2 [75] with $W_{SB}$. For the $3.50\times10^{-3}$ g bed, $V_{pore}$ is $2.4_7$ $\mu$l. The quantity $(V_{HU} - V_{pore})$ is associated with extra-particle void spaces (i.e. $7.6_6$ $\mu$l). This subtraction is made because diffusion of solute into the pores in the particle must be considered as part of the process of sorption.

Sorption-rate measurements employing the recirculation apparatus (Fig. 5) were performed as follows: First, the bed of XAD-2 was flushed for 30 min with a solution of $3.505\times10^{-5}$ mol/l of 4-PADPA in methanol, with the column effluent directed to waste. Although shallow-bed kinetic conditions are not met in the 3-cm long bed at short times (e.g. $\lesssim$1 min) this is of no consequence, since they are met for most of this 30-min period. After 30 min the entire bed has uniformly been brought quite close to equilibrium with the 4-PADPA solution and the sorption rate has become very slow. Next, valve $V_2$ was switched and the solution in the closed-loop was recirculated by the peristaltic pump P2 for a period of time between 30 and 90 min, at the end of which the signal from the detector was measured. Then valve $V_2$ was switched and a fresh amount of the same 4-PADPA solution was again flushed through the system to waste, but only for a few minutes until the absorbance increased by a small amount to a constant value. The difference in detector signal after and before this flushing is related via a suitable calibration curve, to the increase in concentration, $\Delta C_S$, of 4-PADPA that has sorbed onto the XAD-2 during recirculation. This

sequence of recirculation and flushing steps was repeated until $\Delta C_S$ became negligible on a ca. 90-min time scale.

Calculation of $\Delta C_S$ for each cycle of the recirculation experiment is made via the following expression:

$$\Delta C_S = \frac{\Delta C_M V_{loop}}{W_{SB}} \quad (15)$$

where $\Delta C_M$ is the concentration decrease in the solution that occurred during recirculation and $V_{loop}$ is the hold-up (void) volume of the entire recirculation loop. The $\Delta C_S$ increments are cumulatively added to the 30-min value of $C_S$ obtained for the sorption of 4-PADPA from a solution of the same concentration in the shallow-bed experiment. The value of $V_{loop}$ was measured to be 0.849 ml by filling the recirculation loop with a known concentration solution of the unretained compound phloroglucinol and spectrophotometrically determining the moles of phloroglucinol in the loop. Use of the recirculation technique to measure $C_S$ in the nearly flat region of the sorption-rate curve (Fig. 1) provides data having low scatter, which yield a more accurate estimate of the very small slope of the rate curve in this region.

The sorption isotherm of 4-PADPA on XAD-2 was measured in an apparatus that is essentially the same as the one shown in Fig. 3 and Fig. 4. The procedure involved the same steps as those listed for measuring the sorption-rate curve by the shallow-bed method, with the following changes. Sample solutions contained various concentrations of 4-PADPA in the range $3.72\times10^{-6}$ mol/l to $1.48\times10^{-3}$ mol/l in methanol. The sorption time was either 30 or 40 min, at a flow-rate of 1.0 ml/min. Depending on the concentration range involved, the desorbed 4-PADPA either was collected in the holding loop in valve $V_3$ for subsequent rinsing through the detector, or it was collected in a 50-ml volumetric flask and subsequently measured spectrophotometrically. Calculation of $C_S$ was performed via Eq. 14. Although a 30- to 40-min sorption time is inadequate fully to achieve sorption equilibrium, it is nevertheless long enough to achieve >95% equilibration (Fig. 1) and therefore to permit an accurate location of the linear region of the sorption isotherm.

The elution chromatograms on the 51 cm long column of XAD-2 were measured by injecting a $4\times10^{-4}$ mol/l solution of 4-PADPA in methanol, at a methanol-eluent flow-rate of 0.010 ml/min for one hour. The eluent flow-rate was then increased to either 0.106 ml/min or 0.386 ml/min and the timer was started. The volumes of the collected fractions were 7.63 ml and 19.3 ml, respectively. These fraction volumes were established by setting the tube advance times on the fraction collector to 72 min and 50 min. A concentration as high as $4\times10^{-4}$ mol/l was injected in order to be able accurately to quantify the concentrations of 4-PADPA in the effluent from the column. This concentration is

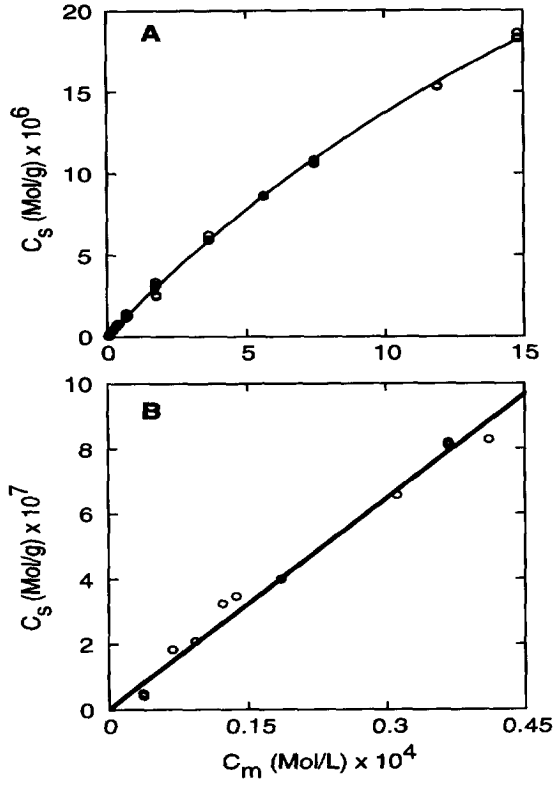


Fig. 6. Sorption isotherm of 4-PADPA measured by column equilibration on the 3.50 mg bed of XAD-2. $C_S$ is sorbed concentration from Eq. 14 and $C_M$ is solution concentration. Circles represent experimental data. The solid line in (A) is a fit of the Langmuir equation to all of the data. The solid line in (B) is a linear fit to the low concentration points from (A).

somewhat above the linear region of the isotherm, as can be seen by comparing the slope of about 0.016 l/g at $C_M = 4 \times 10^{-4}$ mol/l (Fig. 6A) with a slope of 0.0213 l/g in the linear region (Fig. 6B). However, dilution due to bandbroadening on the column quickly lowers the concentration of 4-PADPA, so that the elution chromatograms can be considered to have been performed in the linear region of the isotherm.

The void volume of the column, or retention volume of an unretained component, $V_M$, was measured by weighing the column when it was dry and when it was filled with methanol mobile phase, dividing the weight of methanol in the column by the density of methanol, and subtracting the small extra-column volume of methanol which is present in the column end fittings.

## 4. Results and discussion

Several conditions are implicit in the use of the experimental sorption-rate curve to predict the elution chromatographic peak associated with intra-particle sorption rate: (i) The value of $K_D$ must be independent of solute concentration, which is to say that the concentration of solute must be in the linear part of its distribution isotherm; (ii) the sorption-rate curve must be measured under infinite bath conditions with film diffusion making a negligible contribution to rate control; (iii) the value of $n_0$ obtained from fitting the sorption-rate curve must be the equilibrium value, at least on a time scale that is comparable to the time required for the solute to traverse a "theoretical plate" in the elution chromatogram experiment; (iv) a multi-exponential equation must provide a good fit to the sorption-rate curve. In the discussion below these conditions are addressed along with both the theoretical and experimental results.

### 4.1. Sorption isotherm

Shown in Fig. 6A is a plot of moles of 4-phenylazodiphenylamine sorbed at equilibrium on a $3.50 \times 10^{-3}$ g shallow bed of XAD-2 versus concentration in methanol. The solid line in Fig. 6A is a fit of the Langmuir equation to the data points [14]. No special significance is attached to this: For other systems, both Langmuirian and non-Langmuirian isotherms have been observed on XAD-2 [37,45,76,77]. In Fig. 6B is shown the low-concentration, linear region of the isotherm. From the slope of the straight line which is fit to the first 11 data points, a mass–volume distribution coefficient has the value $0.0213 \pm 0.0008$ l/g. Solution concentrations of $(3–4) \times 10^{-5}$ mol/l which were used in the shallow bed sorption-rate measurements are in the linear region.

### 4.2. Shallow-bed conditions

The shallow-bed rate experiment operates under infinite bath conditions and it can be run under film-diffusion rate control, intra-particle rate control or some combination of both [42–44,47]. In this work it is desired to have exclusively intra-particle rate control. This is favored by employing larger sorbent particle size, higher solute concentration, lower solute $k'$ and higher linear velocity of mobile phase through the shallow bed [16,43]. Since the nature of the solute and its concentration, the nature of the mobile phase, and the size of the particles have all been pre-selected, the linear velocity is the only parameter which can be varied in order to achieve intra-particle rate control. At higher linear velocities the thickness of the Nernst diffusion film decreases, which leads to faster film diffusion [17,18,42,43,46,47,59]. Film diffusion and intra-particle sorption rate occur in series, so that the faster film diffusion becomes, the smaller contribution it makes to rate control. At sufficiently high linear velocities rate control becomes, in effect, exclusively intra-particle [43,45,46].

In order to identify the minimum linear velocity required to achieve, simultaneously, both infinite bath conditions and exclusive intra-particle rate control the sorption-rate experiment was repeated at a series of increasing linear velocities and the resulting initial rates, obtained over the first 0.25 min, were compared with one another. Since film

diffusion is expected to make its greatest contribution very early in the rate experiment [16,43,46,59], and since the rate of removal of solute from the solution is also greatest early in the experiment, initial rates are most sensitive to these effects. Over the first 0.25 min the sorption-rate curves can be approximated as straight lines. The slopes of these straight lines obtained at various flow-rates ($F$, ml/min) and their corresponding interstitial linear velocities ($U_{inter}$, cm/s) are presented in Table 1. The interstitial linear velocity in cm/s is related to the flow-rate in ml/min by the expression:

$$U_{inter} = \frac{F}{\pi r^2 \epsilon_{inter} 60} = \frac{F}{1.44} \quad (16)$$

in which $r$ is the radius of the shallow bed (0.15 cm) and $\epsilon_{inter}$ is the inter-particle porosity of the bed ($\approx 0.3_4$, Ref. [75]). The corresponding numbers of inter-particle bed-volumes passing through the bed per second are also listed in Table 1. It can be seen that the sorption rate becomes constant at $U_{inter} \gtrsim 1.2$ cm/s (i.e. $\gtrsim$9 bed volumes per second), signifying that complete shallow-bed conditions are achieved. Based on this information all subsequent sorption-rate experiments were performed at linear velocities high enough to insure that shallow-bed conditions prevailed.

### 4.3. Sorption-rate curve

As noted above, the solid lines in Fig. 1A and 1B represent the fit of the empirical tri-exponential equation to the data points from the shallow-bed sorption-rate experiments, runs 1 and 2, respectively. For each of Fig. 1A and 1B the six parameters $k_1$, $k_2$, $k_3$, $n_1$, $n_2$, and $n_3$ are fitting parameters which have been adjusted to minimize $\chi^2$ [78,79] via a non-linear least-squares simplex algorithm in a program in the software package Mat-Lab [80]. The equations of these lines are:

$$F = 1 - 0.2846 \exp(-1.818t) - 0.6844 \exp(-0.1916t) - 0.0310 \exp(-0.00251t) \quad (17)$$

for Fig. 1A and,

$$F = 1 - 0.2693 \exp(-1.245t) - 0.7143 \exp(-0.242t) - 0.0164 \exp(-0.000425t) \quad (18)$$

for Fig. 1B. The units of the rate constants $k_j$ in the exponential terms are $min^{-1}$.

A well-known difficulty exists with the curve fitting of multi-exponential equations to experimental data [78,79,81,82]. The presence of scatter in the experimental data creates ambiguities in establishing values for the $n_j$ and $k_j$ parameters. Sensitivity analysis was performed for the fitting of the rate data in Fig. 1A and 1B. This was done by employing a wide variety of initial estimates of the six parameters to be used when initiating the curve fitting program. It was found that the values $n_1$, $n_2$, $k_1$, and $k_2$ which

Table 1
Initial sorption rates over the first 0.25 min on the 3.50 mg bed of XAD-2 as a function of flow-rate and interstitial linear velocity of solution through the bed in order to verify shallow-bed conditions

| $F$ (ml/min) | $U_{inter}$ [a] (cm/s) | No. Bed Vol.[b] per sec | Initial rate (mol/kg/min) |
|---|---|---|---|
| 0.72 | 0.50 | 4 | 4.0×10−4 |
| 1.32 | 0.92 | 7 | 4.4×10−4 |
| 1.68 | 1.17 | 9 | 4.8×10−4 |
| 1.98 | 1.38 | 11 | 4.8×10−4 |
| 3.30 | 2.29 | 18 | 5.0×10−4 |

Uncertainties are implied by significant figures.
[a] $U_{inter}$ is from Eq. 16.
[b] Interstitial (i.e. inter-particle) bed volume is 0.0030 ml.

were returned by the program after convergence varied very little, and that these small variations produced insignificant differences in the elution peaks predicted for hypothetical columns 1 and 2. However, in marked contrast, the values returned for $n_3$ and $k_3$ by the program varied by orders of magnitude when different initial estimates were employed. The parameters are strongly correlated so that an increased value of $k_3$ compensates a decreased value of $n_3$. A large value for $n_3$ means that the true equilibrium value of $C_S$ is much larger than the value observed after 300 min, and the corresponding small value of $k_3$ means that equilibrium will be approached very slowly at a time reached by great extrapolation of the data in the nearly flat region of the rate curve. Such extrapolation to values well beyond the data set is never justified, so that the seeming ambiguity in identifying the "correct" set of $n_3/k_3$ for a given rate curve is readily resolved by applying two simple criteria: The correct set is the one which yields, both, the minimum value of $\chi^2$ (many combinations do) and the smallest value of $n_3$.

A somewhat related point, also resulting from the "sensitivity" of multi-exponential curve fitting, is the fact that all six values of $n_j$ and $k_j$ which describe one rate curve (e.g. Eq. 17 and Fig. 1) differ from those which describe a replicate rate curve (e.g. Eq. 18 and Fig. 1B). This is not a problem, since these parameters are assigned no physical reality, and in fact, the different sets both predict similar overall elution peaks, as discussed later in connection with Table 2.

### 4.4. Observed elution peaks

Shown as data points in Figs. 7A and 8A is the observed chromatographic peak for the elution of 4-PADPA from the 51-cm column of XAD-2 at a mobile phase flow-rate of 0.106 ml/min. Shown as data points in Fig. 8B is the observed chromatographic peak for elution of 4-PADPA at a flow-rate of 0.386 ml/min. Extra-column contributions to both $V_R$ and bandbroadening are negligible since the volumes of the injected sample, of the extra-column tubing and fittings, and of the collected fractions are all much smaller than the widths of the observed peaks.

Quantitative characterization of these observed elution peaks is conveniently performed by statistical moment analysis [83,84]. In order to avoid the baseline-setting errors associated with the calculation of moments directly from the chromatographic data points, the moments have been calculated from the

Table 2
Chromatographic parameters and figures of merit for observed (OBS) and predicted (PRE) elution peaks of 4-PADPA on a 51-cm column of XAD-2

| $F$ (ml/min)/$U_o$[a] (cm/s) | Peak | $V_R$ (ml) | $V_G$[b] (ml) | $V_{exp}$[c] (ml) | $\sigma^2$[d] (ml)$^2$ | $\sigma_G^2$[e] (ml)$^2$ | $\sigma_{exp}^2$[f] (ml)$^2$ | $H$ (mm) | A.F. |
|---|---|---|---|---|---|---|---|---|---|
| 0.106/0.00205 | PRE #1 | 689 | 632 | 57 | $8\times10^3$ | $4\times10^3$ | $3\times10^3$ | 8 | 1.3 |
| | PRE #2 | 683 | 644 | 39 | $6\times10^3$ | $4\times10^3$ | $2\times10^3$ | 6 | 1.2 |
| | Avg. PRE | 686 | 638 | 48 | $7\times10^3$ | $4\times10^3$ | $2\times10^3$ | 7 | 1.2 |
| | OBS | 692 | 610 | 82 | $9\times10^3$ | $2\times10^3$ | $7\times10^3$ | 9 | 1.7 |
| 0.386/0.00747 | PRE #1 | 642 | 538 | 105 | $23\times10^3$ | $12\times10^3$ | $11\times10^3$ | 28 | 1.6 |
| | PRE #2 | 638 | 566 | 72 | $16\times10^3$ | $11\times10^3$ | $5\times10^3$ | 21 | 1.4 |
| | Avg. PRE | 640 | 552 | 88 | $20\times10^3$ | $12\times10^3$ | $8\times10^3$ | 24 | 1.5 |
| | OBS | 652 | 570 | 82 | $12\times10^3$ | $5\times10^3$ | $7\times10^3$ | 15 | 1.5 |

Uncertainties are implied by significant figures.
[a] $U_o$ is from Eq. 19.
[b] $V_G$ is first moment of Gaussian component of EMG representation of peak.
[c] $V_{exp}$ is first moment of exponential component of EMG representation of peak.
[d] $\sigma^2$ is second moment of overall EMG representation of peak.
[e] $\sigma_G^2$ is second moment of Gaussian component of EMG representation of peak.
[f] $\sigma_{exp}^2$ is second moment of exponential component of EMG representation of peak.

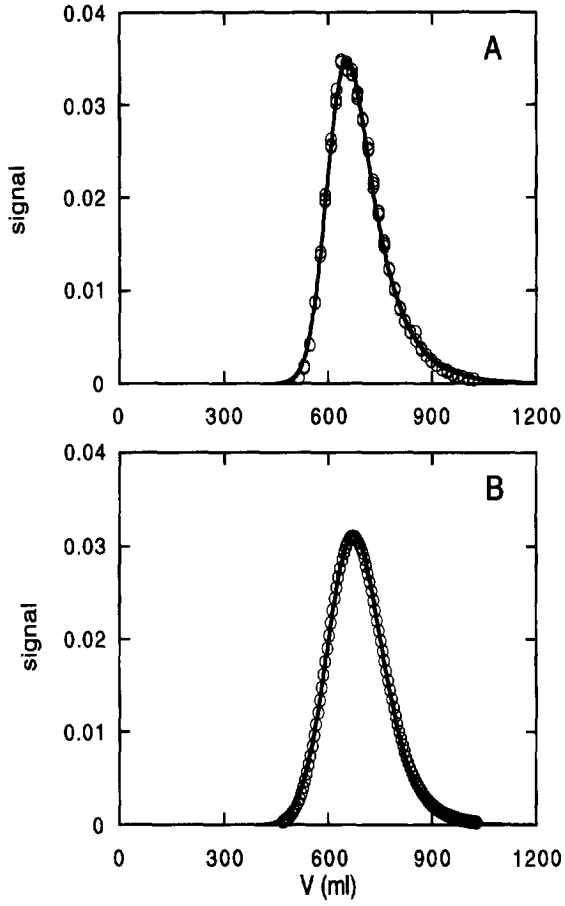


Fig. 7. Exponentially-modified Gaussian (EMG) fit to the observed (A) and predicted (B) chromatograms of 4-PADPA on the 51-cm column of XAD-2 at $F = 0.106$ ml/min. Circles in (A) represent experimental points. The circles in (B) are predicted using rate constants from run 1. The solid lines in both (A) and (B) are the EMG-fit lines.

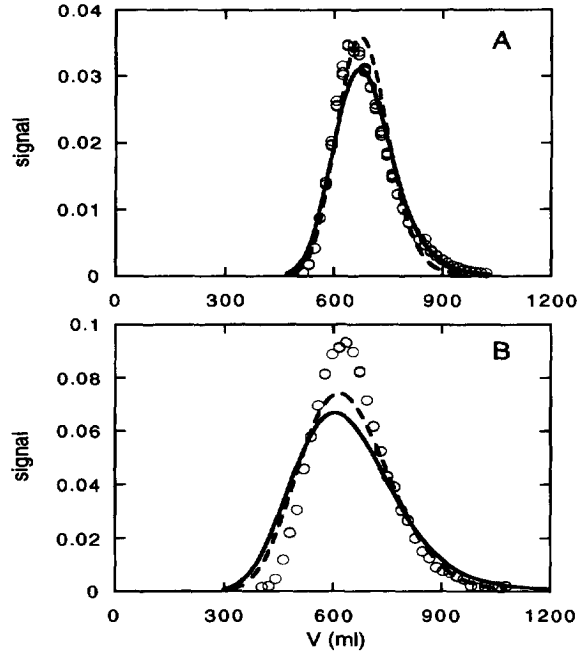


Fig. 8. Comparison of observed and predicted elution chromatograms for 4-PADPA on the 51-cm column of XAD-2 at 0.106 ml/min (A) and 0.386 ml/min (B). Circles are experimental. Solid lines and dashed lines are predicted using constants from kinetic run 1 and run 2, respectively. At a given flow-rate the predicted peaks have the same area as the observed peak.

exponentially-modified Gaussian (EMG) representations of the data [85–87]. The EMG function [62,83,85,88–90] was fit to the experimental points obtained at each of the two flow-rates by means of non-linear least squares. As a typical example, the solid line drawn through the points in Fig. 7A is the EMG fit-line to the data observed at $F = 0.106$ ml/min. An equally good fit was obtained for the data observed at 0.386 ml/min (not shown).

Results of statistical moment analysis of these two EMG fit-lines to the observed chromatograms are summarized in rows 4 and 8 in Table 2. The first moment is the center-of-gravity of the peak in ml, ($V_R = V_G + V_{exp}$); the second moment is its variance in $(ml)^2$, $\sigma^2 = \sigma_G^2 + \sigma_{exp}^2$; and the expression $L\sigma^2/V_R^2$ is the plate height ($H$) of the column [34,88,91]. Here $V_R$ and $\sigma^2$ are the first and second moments of the overall EMG peak; $V_G$ and $\sigma_G^2$ are the first and second moments of the Gaussian component of the peak; and $V_{exp}$ and $\sigma_{exp}^2$ are the first and second moments of the exponential component of the peak. The asymmetry factor A.F. is measured at one tenth of the peak height [87,88,92] on the observed peaks which are shown in Fig. 8, not on their EMG fit lines. The moments, the plate height and the asymmetry factor serve as figures of merit for a peak.

In the first column of Table 2 are given the two flow-rates employed in the chromatography, as well as the corresponding linear velocities of the mobile phase $U_o$. The latter in cm/s are related to the former in ml/min by the expression:

$$U_o = \frac{F}{\pi r^2(\epsilon_{inter} + \epsilon_{intra})60} \quad (19)$$

in which $r = 0.63_5$ cm, $\epsilon_{inter} = 0.3_4$ ml/ml and $\epsilon_{intra} = 0.23$ ml/ml.

Comparison of the figures of merit of the observed peak at 0.386 ml/min (0.00747 cm/s) with those of the observed peak at 0.106 ml/min (0.00205 cm/s) shows that both the overall variance ($\sigma^2$) and the plate height ($H$) increase with increasing linear velocity, as expected for a peak whose bandbroadening arises exclusively from intra-particle rate processes. In terms of the EMG representation, the increase in $\sigma^2$ is due to an increase in the Gaussian component ($\sigma_G^2$), rather than to the exponential component ($\sigma_{exp}^2$). However, as discussed below, the relative contributions of $\sigma_G^2$ and $\sigma_{exp}^2$ to $\sigma^2$ are very sensitive to small differences in peak shape, so that this apparent lack of dependence of $\sigma_{exp}^2$ on $U_o$ is not highly significant. The observed asymmetry factor decreases at higher $U_o$, but here too, a small difference (e.g. 0.2) represents a relatively small change in peak shape.

### 4.5. Predicted elution peaks

Shown as lines in Fig. 8A and 8B are the chromatographic elution peaks that are predicted by the approach outlined in the Theory section for 4-PADPA on the 51-cm column of XAD-2. The solid-line peaks are predicted using the adsorption and desorption-rate constants from the kinetic run 1; and the dashed-line peaks are predicted from the rate constants from run 2. The relevant rate constants $k_{a,j}$ and $k_{d,j}$ are presented in columns 5 and 6 in Table 3. The capacity factors $k'$ in Table 3 were calculated from Eq. 12 using as $V_R$ the first moments of the observed elution peaks at the corresponding flow-rates (i.e. $V_R$ values from rows 4 and 8 in Table 2).

For consistency when comparing predicted with observed peaks, the predicted peaks in Fig. 8A and 8B were fit by the EMG function. This function is not shown in Fig. 8, but it is shown for $F = 0.106$ ml/min as the solid line fit to the theoretically predicted points in Fig. 7B. An equally good fit by the EMG function was found, but is not shown, for the predicted peak at $F = 0.386$ ml/min. It should be noted that the solid line in Fig. 8A, the points in Fig. 7B and the solid line in panel K of Fig. 2 all represent the same predicted elution peak which was calculated from the rate constants obtained in kinetic run 1.

Quantitative characterization of the predicted elution peaks has been performed in terms of the

Table 3
Adsorption and desorption rate constants for hypothetical columns $j = 1$, 2 and 3 based on sorption-rate experiments

| $F$ (ml/min) | $V_R$[a] (ml) | $k'$[b] | $j$ | $k_{a,j}$[c] ($min^{-1}$) | $k_{d,j}$[c] ($min^{-1}$) | exp ($-k_{a,j}t_M$)[d] |
|---|---|---|---|---|---|---|
| 0.106 | 692 | 15.0 | 1 | 1.47/1.00 | 0.345/0.247 | $<10^{-10}/<10^{-10}$ |
| | | | 2 | 0.175/0.221 | 0.017/0.0207 | $<10^{10}/<10^{10}$ |
| | | | 3 | $8.0\times10^{-4}/0.84\times10^{-4}$ | $17\times10^{-4}/3.4\times10^{-4}$ | 0.72/0.97 |
| 0.386 | 652 | 14.1 | 1 | 1.45/0.98 | 0.364/0.260 | $<10^{-10}/<10^{-10}$ |
| | | | 2 | 0.174/0.220 | 0.018/0.0219 | $3\times10^{-9}/<10^{-10}$ |
| | | | 3 | $7.6\times10^{-4}/0.79\times10^{-4}$ | $17\times10^{-4}/3.5\times10^{-4}$ | 0.92/0.99 |

Data are reported as, for example, $k_{a,j}$ (from run 1)/$k_{a,j}$ (from run 2) at the same flow-rates and $V_R$ as for the observed elution peaks. Uncertainties are implied by significant figures.

[a] $V_R$ from rows 4 and 8 in Table 2.

[b] $k'$ is from Eq. 12.

[c] Rate constants are from Eqs. 4 to 9.

[d] This exponential term is the fraction of solute never sorbed; from Eq. 10.

statistical moments of their EMG functions and in terms of their asymmetry factors A.F. The moments and other figures of merit are summarized in rows 1 to 3 and 5 to 7 of Table 2, with the values in rows 3 and 7 being the averages of the predicted (PRE) results obtained using the rate constants from runs 1 and 2.

An important characteristic of the representation of a chromatogram by the EMG function is revealed by comparing the two curves predicted at a given flow-rate with one another. Visually the dashed line and the solid line are quite close to one another as are their plate heights (e.g. 28 vs. 21 at 0.386 ml/min). However, the relative contributions of $\sigma_G^2$ and $\sigma_{exp}^2$ to $\sigma^2$ may vary considerably between the dashed and solid predicted curves (e.g. 12/11 vs. 11/5 at 0.386 ml/min). That is, the "division" of a chromatographic peak into a Gaussian and an exponential component, in the EMG representation, is quite sensitive to small differences in the peak shape.

### 4.6. Accuracy of predicted peaks

In Fig. 8 it can be seen by eye that the predicted peak (either the solid or the dashed line) seems to be a good representation of the observed peak (data points). In Fig. 8B the agreement between the predicted and observed peaks seems to the eye to be reasonable, but not as good as for Fig. 8A. Comparison of the figures of merit $\sigma^2$, $\sigma_G^2$, $\sigma_{exp}^2$ and $H$, at a given flow-rate reveals that they are all quite sensitive to what appears to the eye to be relatively small differences in shape. This reflects in part the general problem of obtaining an accurate quantitative characterization of a peak which exhibits significant asymmetry; even after the situation has been improved by employing the EMG fitting function.

Compared to $\sigma$ and $H$, the asymmetry factor at 10% of peak height, A.F. can be even more sensitive to small differences among peaks which exhibit the kind of "kinetic tailing" [67] that is evident in Fig. 8. In this type of tailing the trailing edge of the peak, just above the baseline, is especially drawn out so that its exact shape is difficult to ascertain. In this connection, it should be noted that these inaccuracies in quantifying asymmetry are just as great for the predicted peak as they are for the observed peak. This is because the small amount of scatter which is present in the data on the plateau of the sorption-rate curve introduces the same uncertainty in defining the predicted peak shape as the scatter of the data on the tail of the observed peak creates in defining its shape.

The question of identifying a set of meaningful quantitative criteria for the "goodness of fit" of the predicted peaks to the observed peaks in Fig. 8 is complicated by the ambiguities in characterizing asymmetric peaks. In contrast, for symmetric, Gaussian-shaped peaks these ambiguities do not exist. In the Gaussian case the standard deviation of the overall peak, $\sigma$ (i.e., the square root of the second moment), is equal to the standard deviation of the Gaussian component $\sigma_G$, so that $\sigma$ is directly proportional to the peak width at any specified fraction of peak height. Thus, for the Gaussian case, comparison of a predicted peak with an observed peak, when they have the same center-of-gravity, $V_R$, is conveniently and simply accomplished by comparing their standard deviation or, equivalently, by comparing the square roots of their plate heights, $H^{1/2}$.

Since the peaks in Fig. 8 are not grossly asymmetric, a reasonable set of criteria for the "goodness of fit" of the predicted to the observed peak is obtained by employing both $H^{1/2}$ and the asymmetry factors. In Fig. 8A, $H^{1/2}$ for the observed peak (i.e., $9^{1/2}$) is only 13% larger than $H^{1/2}$ for the average predicted peak (i.e., $7^{1/2}$). The asymmetry factor is 29% smaller for the predicted peak than for the observed. For the results observed at the higher flow-rate, shown in Fig. 3B, $H^{1/2}$ for the observed peak is 21% smaller than $H^{1/2}$ for the average predicted peak, while there is close agreement between observed and predicted peak for A.F. In general, the agreement between predicted and observed peak shapes is quite acceptable at both flow-rates.

## 5. Conclusions

These experiments were performed using very large particles and small $U_o$ so that intra-particle effects would be the only significant bandbroadening

process. The agreement of the predicted with the observed peaks demonstrates the validity of the proposed approach to predicting the contribution of intra-particle sorption rate to chromatographic bandbroadening. The large plate heights, both observed and predicted, for the chromatography of 4-PADPA in methanol on XAD-2 confirms earlier suggestions that the poor column efficiency which is sometimes observed on porous-polymer sorbents arises from slow intra-particle processes. The slowness of these processes can be appreciated by noting that the plate heights of 9 and 15 mm seen in the observed (OBS) chromatograms at linear velocities of 0.00205 cm/s and 0.00745 cm/s correspond to reduced plate heights of 26 and 42 at reduced linear velocities of ≈16 and ≈59, respectively [93]. Also, the slowness of these processes can be appreciated by comparing the plate heights in Table 2 with those that would be expected from the phenomenon of "resistance to mass transfer in the stagnant mobile phase". This plate height, $H_{SM}$, may be estimated from Eq. 1 using typical parameter values of 0.06 for the "constant" for a solute with $k' = 14$, and $5 \times 10^{-6}$ $cm^2/s$ for $D$ [53], along with 0.036 cm for dp for XAD-2. The expected peaks would be Gaussian and their expected plate heights from Eq. 1 are $H_{SM} \approx 0.3$ mm at $U_o = 0.00205$ cm/s and $H_{SM} \approx 1.3$ mm at $U_o = 0.00745$ cm/s, which are at least an order of magnitude smaller than the values in Table 2.

The proposed approach to predicting peak shape is not limited to porous polymers or to slow intra-particle sorption rates. Of course, faster rates require "shallower" beds and higher flow velocities in order to achieve shallow-bed conditions. In this laboratory, it has been successfully applied to a commercially available 10-$\mu$m diameter spherical PS–DVB, HPLC packing. These results are subject of Part II of this series [94].

## Acknowledgments

This work was supported by the Natural Sciences and Engineering Research Council of Canada and by the University of Alberta.

## References

[1] D.J. Pietrzyk, in P.R. Brown and R.A. Hartwick (Editors), High Performance Liquid Chromatography (Chem. Anal.), Vol. 98, Wiley, New York, 1989, Ch. 10.
[2] R.L. Albright, Reactive Polymers, 4 (1986) 155.
[3] F. Nevejans and M. Verzele, J. Chromatogr., 406 (1987) 325.
[4] F. Nevejans and M. Verzele, Chromatographia, 20 (1985) 173.
[5] D.P. Lee, J. Chromatogr., 443 (1988) 143.
[6] IUPAC, Manual of Symbols and Terminology, Appendix 2, Part I, Pure Appl. Chem., 31 (1972) 578.
[7] K. Unger, Porous Silica, J. Chromatogr. Library, Vol. 16, Elsevier, 1979, Ch. 2.
[8] J. Seidl, J. Malinsky, K. Dusek and W. Heitz, Adv. Polymer Sci., 5 (1967) 113.
[9] K. Kun and R. Kunin, J. Polymer Sci. Part A.1, 6 (1968) 2689.
[10] J.R. Benson and D.J. Woo, J. Chromatogr. Sci., 22 (1984) 386.
[11] R.M. Smith and D.R. Garside, J. Chromatogr., 407 (1987) 19.
[12] W.R. Melander and C. Horvath, in C. Horvath (Editor), High Performance Liquid Chromatography: Advances and Perspectives, Vol. 2, Academic Press, New York, 1980, Chapter 3.
[13] D. Liru, H. Xizhang, W. Quhui, M. Qingcheng, L. Yuliang and Z. Youliang, Scientia Sinica (Series B), 25 (1982) 905.
[14] R.L. Gustafson, R.L. Albright, J. Heisler, J.A. Lirio and O.T. Reid, Jr., Ind. Eng. Chem. Prod. Res. Dev., 7 (1968) 107.
[15] J.C. Giddings, Dynamics of Chromatography, Dekker, New York, 1965.
[16] F. Helfferich, Ion Exchange, McGraw-Hill, New York, 1962, Chapters 6 and 9.
[17] C. Horvath and H.J. Lin, J. Chromatogr., 126 (1976) 401.
[18] W.I. Weber, in A.L. Myers and G. Belfort (Editors), Fundamentals of Adsorption, Engineering Foundations, 1983, pp. 679–692.
[19] D.D. Frey, E. Schweinheim and C. Horvath, Biotechnol. Prog., 9 (1993) 273.
[20] M. Suzuki, Adsorption Engineering, Elsevier, Amsterdam, 1990, Chapters 4–7.
[21] D.M. Ruthven, Principles of Adsorption and Adsorption Processes, Wiley, New York, 1984, Chapters 5 and 6.
[22] J.C. Giddings, Dynamics of Chromatography, Dekker, New York, 1965, Chapters 2 and 6.
[23] R.G. Peel and A. Benedek, J. Environ. Eng. Div. Am. Civil Eng., 106 (EE4) (1980) 797.
[24] J.M. Smith, in W.J. Weber, Jr. and E. Matijevic (Editors), Adsorption from Aqueous Solution, ACS Symp. Ser., Vol. 79, American Chemical Society, Washington, DC, 1968, pp. 8–22.
[25] A.M. Lenhoff, J. Chromatogr., 384 (1987) 285.
[26] J.C. Chen and S.G. Weber, Anal. Chem., 55 (1983) 127.
[27] J.P. Crombeen, H. Poppe and J.C. Kraak, Chromatographia, 22 (1986) 319.

[28] J.C. Giddings, L.M. Bowman and M.N. Myers, Macromolecules, 10 (1977) 443.
[29] J.K. Barr and D.T. Sawyer, Anal. Chem., 36 (1964) 1753.
[30] R. Groh and I. Halasz, Anal. Chem., 53 (1981) 1325.
[31] J.R. Conder and C.L. Young, Physicochemical Measurement by Gas Chromatography, Wiley, New York, 1979, Chapter 12.
[32] C. Horvath and H.J. Lin, J. Chromatogr., 149 (1978) 43.
[33] D.M. Ruthven, in A.E. Rodrigues, M.D. LeVan and D. Tondeur (Editors), Adsorption Sci. Technol.: NATO Adv. Study Inst. on Adsorption: Sci. Technol. Proceedings, Vol. 158, Kluwer Academic Publishers, Boston, MA, 1988, pp. 87–114.
[34] D.B. Marshall, J.W. Burns and D.E. Connolly, J. Chromatogr., 360 (1986) 13.
[35] S.W. Waite, D.B. Marshall and J.M. Harris, Anal. Chem., 66 (1994) 2052.
[36] E.D. von Meerwall, J. Non-Cryst. Solids, 131–132 (1991) 735.
[37] C. Sarzanini, V. Porta and E. Mentasti, New J. Chem., 13 (1989) 463.
[38] H.A. Chase, J. Chromatogr., 297 (1984) 179.
[39] R.L. Dedrick and R.L. Beckman, in L.N. Canjar and J.A. Kostecki (Editors), Physical Adsorption Processes and Principles, Chem. Eng. Progress Symp. Series, 63 (1967) 68.
[40] W. Haller, J. Chromatogr., 32 (1968) 676.
[41] C. Costa and A. Rodrigues, in A.L. Myers and G. Belforte (Editors), Fundamentals of Adsorption, Engineering Foundations, 1983, pp. 163–174.
[42] D. Reichenberg, J. Am. Chem. Soc., 75 (1953) 589.
[43] G.E. Boyd, A.W. Adamson and L.S. Myers, J. Am. Chem. Soc., 69 (1947) 2836.
[44] P.A. Riveros and W.C. Cooper, Solv. Ext. Ion Exchange, 6 (1986) 479.
[45] A.A. Aguwa, J.W. Patterson, C.N. Haas and K.E. Noll, J. Water Pollut. Control Fed., 56 (1984) 442.
[46] P. Cornel, H. Sontheimer, R.S. Summers and P.V. Roberts, Chem. Eng. Sci., 41 (1986) 1801.
[47] J.S. Dranoff and L. Lapidus, Ind. Eng. Chem., 53 (1961) 71.
[48] J. Crank, The Mathematics of Diffusion, Oxford University Press, London, 1975, Chapters 6 and 14.
[49] M.N. Goltz and P.V. Roberts, Contaminant Hydrology, 1 (1986) 77.
[50] H. Komiyama and J.M. Smith, Am. Inst. Chem. Eng. J., 20 (1974) 728 and 1110.
[51] B. Lin, S. Golshan-Shirazi and G. Guiochon, J. Phys. Chem., 93 (1989) 3363.
[52] S. Golshan-Shirazi, B.C. Lin and G. Guiochon, J. Phys. Chem., 93 (1989) 6871.
[53] B.L. Karger, L.R. Snyder and C. Horvath, An Introduction to Separation Science, Wiley, New York, 1973, Chapter 5.
[54] E. Ruckenstein, A.S. Vadyanathan and G.R. Youngquist, Chem. Eng. Sci., 26 (1971) 1305.
[55] R.G. Peel and A. Benedek, Environ. Sci. Technol., 14 (1980) 66.
[56] R.G. Peel and A. Benedek and C.M. Crow, Am. Inst. Chem. Eng., 27 (1981) 26.
[57] J.T. Hsu and T. Chen, J. Chromatogr., 404 (1987) 1.
[58] J.C. Crittenden and D.W. Hand, in A.L. Myers and G. Belfort (Editors), Fundamentals of Adsorption, Engineering Foundations, 1983, pp. 185–194.
[59] M.L. Brusseau and P.S.C. Rao, CRC Crit. Rev. in Environmental Contamination, 19 (1989) 33.
[60] J. Villermaux, J. Chromatogr., 406 (1987) 11.
[61] W.A. Beverloo, G.M. Pierik and K.C.A. Luyben, in A.L. Myers and G. Belfort (Editors), Fundamentals of Adsorption, Engineering Foundations, 1983, pp. 95–104.
[62] G.C. Courval and D.G. Gray, Macromolecules, 8 (1975) 916.
[63] B.M. van Vliet, W.J. Weber, Jr. and H. Hozumi, Water Res., 14 (1980) 1719.
[64] J.C. Giddings, Dynamics of Chromatography, Dekker, New York, 1965, Chapter 3.
[65] D.G. Gray and J.E. Guillet, Macromolecules, 7 (1974) 244.
[66] J.C. Giddings and H. Eyring, J. Phys. Chem., 59 (1955) 416.
[67] J.C. Giddings, Anal. Chem., 35 (1963) 1999.
[68] G.N. Watson, Theory of Bessel Functions, Cambridge University Press, 1944.
[69] J. Villermaux, J. Chromatogr. Sci., 12 (1974) 822.
[70] D.A. McQuarrie, J. Chem. Phys., 38 (1963) 437.
[71] G.J.S. Vint and C.S.G. Phillips, J. Chromatogr., 292 (1984) 263.
[72] R.G. Baum, R. Saetre and F.F. Cantwell, Anal. Chem., 52 (1980) 15.
[73] L. Fossey and F.F. Cantwell, Anal. Chem., 54 (1982) 1693.
[74] L.R. Snyder and J.J. Kirkland, Introduction to Modern Liquid Chromatography, Wiley, New York, 1974, Section 6.4.
[75] Amberlite XAD-2, Technical Bulletin, Rohm and Haas Co., Philadelphia, PA, 1972.
[76] R.L. Gustafson and J. Paleos, in S.J. Faust and J.V. Hunter (Editors), Organic Compounds in Aquatic Environments, Dekker, New York, 1971, Chapter 10.
[77] J.L. Lundgren and A.A. Schilt, Anal. Chem., 49 (1977) 974.
[78] C.H. Lochmuller, A.S. Colborn, M.L. Hunnicutt and J. Harris, J. Am. Chem. Soc., 106 (1984) 4077.
[79] P.R. Bevington, Data Reduction and Error Analysis for the Physical Sciences, McGraw-Hill, New York, 1969, Chapter 11.
[80] MATLAB™, The Mathworks, Inc., Natick, MA.
[81] D.B. Marshall, Anal. Chem., 61 (1989) 660.
[82] S.W. Provencher, J. Chem. Phys., 64 (1976) 2272.
[83] O. Sternberg, in Advances in Chromatography, Dekker, New York, Vol. 2, 1966, Chapter 6.
[84] O. Grubner, in Advances in Chromatography, Dekker, New York, Vol. 6, 1986, pp. 173–209.
[85] D.J. Anderson and R.R. Walters, J. Chromatogr. Sci., 22 (1984) 353.
[86] S.M. Chesler and S.P. Cram, Anal. Chem., 43 (1971) 1922.
[87] S.M. Chesler and S.P. Cram, Anal. Chem., 44 (1972) 2240.
[88] J.P. Foley and J.G. Dorsey, Anal. Chem., 55 (1983) 730.
[89] J.P. Foley and J.G. Dorsey, J. Chromatogr. Sci., 22 (1984) 40.
[90] W.W. Yau, Anal. Chem., 49 (1977) 395.

[91] B.A. Bidlingmeyer and F.V. Warren, Anal. Chem., 56 (1984) 1586A.
[92] J.J. Kirkland, W.W. Yau, H.J. Stoklosa and D.H. Dilks, Jr., J. Chromatogr. Sci., 15 (1977) 303.
[93] J.H. Knox, J. Chromatogr. Sci., 15 (1977) 352.
[94] J. Li, L.M. Litwinson and F.F. Cantwell, J. Chromatogr. A, 726 (1996) 25.